Available online at www.sciencedirect.com
ScienceDirect
Trans. Nonferrous Met. Soc. China 34(2024) 861−873
Transactions of Nonferrous Metals Society of China
www.tnmsc.cn

Performance optimization of ternary Ti−Nb−Cu shape memory alloys based on d electron theory

Xiao-yang YI[1], Xin-jian CAO[2], Bo-wen HUANG[3], Kui-shan SUN[3], Bin SUN[4], Xiang-long MENG[3], Zhi-yong GAO[3], Hai-zhen WANG[1]

1. College of Nuclear Equipment and Nuclear Engineering, Yantai University, Yantai 264005, China;
2. Shandong Laboratory of Yantai Advanced Materials and Green Manufacturing, Yantai 264005, China;
3. School of Materials Science and Engineering, Harbin Institute of Technology, Harbin 150001, China;
4. Center of Testing and Analysis, College of Materials Science and Chemical Engineering, Harbin Engineering University, Harbin 150001, China

Received 19 August 2022; accepted 31 December 2022

Abstract: The phase constituents of Ti−Nb−Cu shape memory alloys were designed based on d electron theory, in order to optimize their performances. The XRD analysis and TEM observation revealed that Cu addition led to the reduction of the bond order ($\overline{Bo}$) and metal d-orbital energy level ($\overline{Md}$), which caused the evolution of phase constituents. With increasing Cu content, the variation of phase constituents can be concluded as follows: $\beta+\alpha''\rightarrow\beta+\omega\rightarrow\beta+\alpha''+\omega\rightarrow\beta$. The yield strength, ultimate tensile strength and elongation of Ti−Nb−Cu shape memory alloys firstly increased and then decreased with increasing Cu contents. By optimizing the content of Cu alloying element, Ti−Nb−Cu shape memory alloys possess superior mechanical properties with yield strength of 528 MPa and ultimate tensile strength of 742 MPa, which can mainly be attributed to the comprehensive effect of solution strengthening and grain refinement as well as precipitation strengthening.

Key words: d electron theory; Ti−Nb−Cu shape memory alloy; martensite configuration; tensile properties; microhardness

1 Introduction

Compared with binary Ti−Ni shape memory alloys, β-type Ti-based shape memory alloys have become the most promising candidates for biomedical shape memory alloys due to various advantages such as lower elastic modulus, excellent biocompatibility, high corrosion resistance, non-toxicity and good cold workability [1−3]. The functional performances including shape memory effect and superelasticity for β-type Ti-based shape memory alloys are originated from the reversible $\beta\rightleftharpoons\alpha''$ martensite transformation [4,5]. Recently, primary β-Ti-based shape memory alloys consist of Ti−Nb [6], Ti−Mo [7], Ti−Cr [8], Ti−Au [9] and Ti−Cr [10] etc. Particularly, there has been tremendous progress in developing Ti−Nb-based shape memory alloys in the past decade. For instance, the microstructural features, martensitic transformation behaviors, mechanical properties and shape memory effect or superelasticity of Ti−Nb-based shape memory alloys have been extensively studied [11,12]. It is found that the small transformation strain and low strength are two major drawbacks of binary Ti−Nb shape memory alloys [13]. Especially, developing β-type Ti-based shape memory alloys with a lower Young's

Corresponding author: Xiang-long MENG, Tel: +86-451-86412505, E-mail: xlmeng@hit.edu.cn;
Hai-zhen WANG, Tel: +86-18853587031, E-mail: sleepsid@163.com
DOI: 10.1016/S1003-6326(23)66439-8

modulus and higher strength is necessary for the replacement of human bone [14]. However, recent researches have shown that the intrinsic problem of small transformation strain, low Young's modulus and strength of Ti−Nb-based shape memory alloys can be solved by adding alloying elements and controlling microstructure [15]. The Young's modulus and mechanical properties of β-Ti based shape memory alloys change, as the phase constituents are distinctive. The Young's moduli of different phases in most Ti-based shape memory alloys decrease as follows: ω phase > α' martensite phase > α'' martensite phase > β phase [16]. However, the phase compositions of Ti-based shape memory alloys can be evaluated by $\overline{Bo}-\overline{Md}$ diagram ($\overline{Bo}$ is the bond order and $\overline{Md}$ is the metal d-orbital energy level) diagram [17]. This implies that the $\overline{Bo}-\overline{Md}$ diagram can be used for designing the biomedical Ti-based alloys and predicting the functional performances based on the d electron theory. For example, the bio-implant β-Ti shape memory alloys mainly appear in the neighborhood of two parameters, $\overline{Bo}$=2.87 and $\overline{Md}$=2.45 in the $\overline{Bo}-\overline{Md}$ diagram [18]. In addition, the Ti−12Ta−9Nb−3V−6Zr−1.5O and Ti−23Nb−0.7Ta−2Zr−1.2O gum metals shape memory alloys have been optimized based on the $\overline{Bo}-\overline{Md}$ diagram [17]. They not only possess good cold working, but also show superelasticity and ultra-low elastic modulus. Hence, designing the values of $\overline{Bo}$ and $\overline{Md}$ in β-Ti shape memory alloys by controlling alloying elements is an effective method to improve the mechanical and functional properties.

It has been reported that Cu element plays a great important role in the development of biomedical alloys [19]. For instance, Cu can enhance the mechanical properties owing to the solution strengthening mechanism or dispersion strengthening mechanism [20]. Moreover, proper addition of Cu can also improve the bio-corrosion properties and provide strong antibacterial activity [21,22]. Besides, Cu addition also can endow with the new biological functions, such as stimulating proliferation and differentiation of osteoblasts and angiogenesis of endothelia cells, inhibiting the proliferation of vascular smooth muscle cells (VSMC) and promoting the proliferation of vascular endothelial cells (VEC) [19]. This means that Cu addition can promote the biomedical application of Ti−Nb shape memory alloys. Nevertheless, there are few investigations on the microstructure, martensitic transformation and mechanical properties of Ti−Nb−Cu shape memory alloys.

Hence, the ternary Cu element was adopted to tailor the phase constituents to further obtain the Ti−Nb biomedical shape memory alloys with high performances in the present study. At the same time, the relationships between the Cu content and micro-structural features, mechanical properties of Ti−Nb based shape memory alloys were established. The mechanisms for achieving the high performances of Ti−Nb-based shape memory alloys are clarified.

2 Experimental

2.1 Materials preparation

$(Ti-16Nb)_{100-x}-Cu_x$ (x=0.5, 1.0, 1.5, 2.0, 3.0, and 5.0 at.%) shape memory alloy ingots with a mass of 60 g were melted in an arc-melting furnace under the argon atmosphere. For homogenization, all Ti−Nb−Cu shape memory alloy ingots were solution-treated at 900 °C for 24 h under vacuum condition. The homogenized samples were hot-rolled into sheets with a thickness of 4 mm followed by the cold-rolling. The total reduction rate of cold rolling was 75%. The specimens with suitable sizes were prepared by spark-cutting for the following characterization. Then, they were sealed into the vacuum quartz tubes and solution-treated at 900 ℃ for 3 h followed by ice-water quenching.

2.2 Samples characterization

Crystal structures of the Ti−Nb−Cu shape memory alloys were examined by adopting X-ray diffraction spectrometer (XRD, Bruker Discover D8) at room temperature and 2θ=30°−80° using Cu K_α radiation. The microstructure was observed by optical microscope and transmission electron microscope (TEM). For optical observation, the specimens were mechanically polished and etched in a solution composed of 10 vol.% HF + 40 vol.% HNO_3 + 50 vol.% H_2O. TEM observations were carried out using a Talos F200X electron microscope operated at 200 kV. Specimens for TEM observation were prepared by twin jet-polishing in a solution of 6 vol.% perchloric acid, 60 vol.% methyl alcohol and 34 vol.% n-butyl alcohol. Tensile tests were performed at room temperature on an MTS880 machine with an initial strain rate of 0.2 mm/min.

The tensile samples were prepared by spark-cutting parallel to the rolling direction with a gage length of 45 mm. Tensile fracture surface morphologies were observed by means of scanning electron microscope (SEM, ZEISS EVO MA10). The microhardness (HV) measurements were performed on a micro-Vicker hardness tester. The applied loading and duration were 50 g and 10 s, respectively. The microhardness values were evaluated by the average value of at least ten different regions after excluding the highest and lowest values. The specimens for microhardness tests were mechanically polished using 400# SiC papers, until approximately 20 μm depth from the rolling surface was removed. Then, 800# → 1200# → 2000# → 3000# SiC papers were used for finer polishing to obtain a mirror surface.

3 Results and discussion

3.1 Microstructure

Figure 1 shows the XRD patterns of the solution-treated Ti−Nb−Cu shape memory alloys with various Cu contents. Obviously, the phase constituents of Ti−Nb−Cu shape memory alloys are closely related to the Cu content. Single β phase with a cubic structure corresponding to the primary peaks of (110), (200) and (211) is observed in Ti−Nb−Cu shape memory alloys, as Cu content is 1.0 at.%, 3.0 at.% and 5.0 at.%, respectively. While the phase constituents of other Ti−Nb−Cu shape memory alloys with Cu contents of 0.5 at.%, 1.5 at.% and 2.0 at.% consist of predominant β phase and a small amount of orthorhombic α'' martensite. It has been reported that Ti−16Nb shape memory alloys are in martensitic state at room temperature [11]. This indicates that Cu element belongs to the β-stabilizing element, which can promote to the formation of β phase. The similar conclusions have been drawn in other β-Ti shape memory alloys [20,23].

It is calculated from Fig. 1 that the lattice constants of Ti−Nb−Cu shape memory alloys are different as the Cu content changes, which are shown in Fig. 2. The lattice constant of β parent phase (a_o) for Ti−Nb-based shape memory alloys increases with Cu content increasing from 0.5 at.% to 3.0 at.%; whereas a slight drop occurs in Ti−Nb-based shape memory alloys with 5.0 at.% Cu. The lattice constants of α'' martensite phase in Ti−Nb-based shape memory alloys with 1.5 at.% and 2.0 at.% Cu are different, which are respectively as follows: a=3.1197 Å, b=4.6608 Å, c=4.7766 Å; a=3.1203 Å, b=4.7786 Å, c=4.7008 Å. In proportion, the lattice volume of β parent phase first increases and then decreases as Cu content increases from 0.5 at.% to 5.0 at.%. Similarly, the lattice volume of

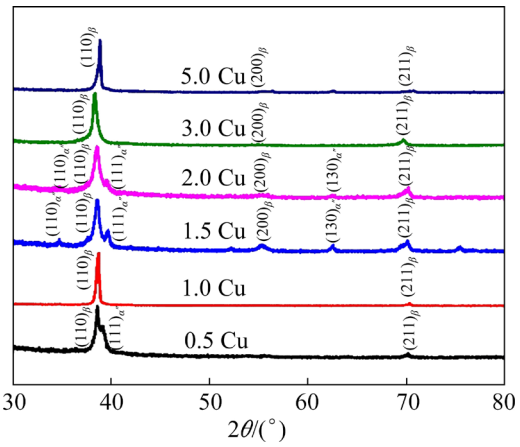

Fig. 1 Room temperature XRD patterns of Ti−Nb−Cu shape memory alloys with various Cu contents

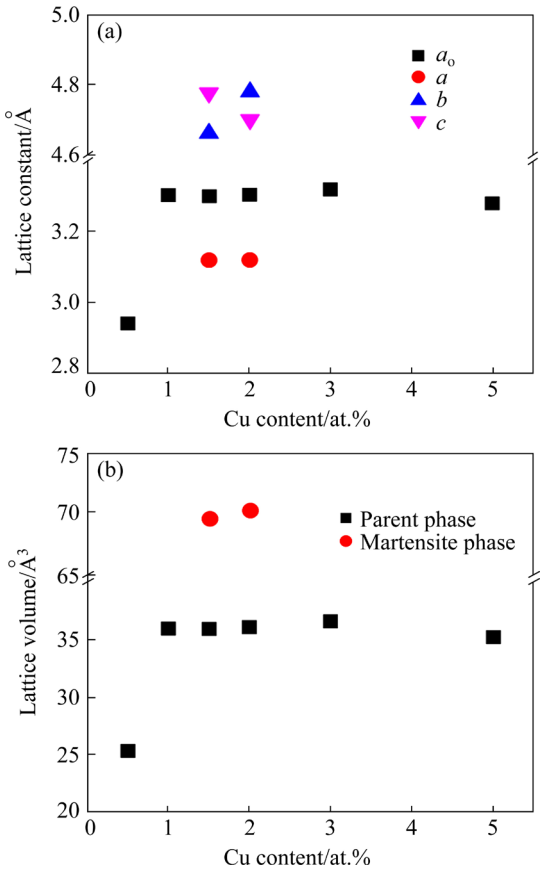

Fig. 2 Effect of Cu content on lattice constants (a) and lattice volume (b) of Ti−Nb−Cu shape memory alloys

α'' martensite phase in Ti−Nb−$Cu_{2.0}$ shape memory alloy is larger than that of Ti−Nb−$Cu_{1.5}$ shape memory alloy. The evolution of lattice constants of Ti−Nb−Cu shape memory alloy with increasing the Cu content can be ascribed to different degrees of lattice distortion induced by different Cu contents dissolving into Ti−Nb matrix.

Figure 3 exhibits the optical images of Ti−Nb−Cu shape memory alloys with different Cu contents. The microstructural features of Ti−Nb−Cu shape memory alloys with various Cu contents are obviously different. Nevertheless, the optical images of Ti−Nb−Cu shape memory alloys are well consistent with the XRD patterns. The featureless β parent phase is found in all Ti−Nb−Cu shape memory alloys, regardless of Cu contents. However, the lath-like α'' martensite phase can also be observed in Ti−Nb−Cu shape memory alloys with 0.5 at.%, 1.5 at.% and 2.0 at.% Cu. The differences are that the martensite lath mainly distributes along the grain boundary in Ti−Nb−Cu shape memory alloys with 0.5 at.% and 2.0 at.% Cu, while the complete martensite lath crosses through the whole grain in Ti−Nb−Cu shape memory alloys with 1.5 at.% Cu.

In addition, the average grain size is obtained from the optical images. The previous studies have shown that the grain size is largely dependent on the composition and processing history of Ti−Nb-based alloys [24−27]. In the present Ti−Nb−Cu shape memory alloys, the Cu content also plays an important role in grain size of Ti−Nb−Cu shape memory alloys, as shown in Fig. 4. With increasing the Cu content, the average grain size first increases

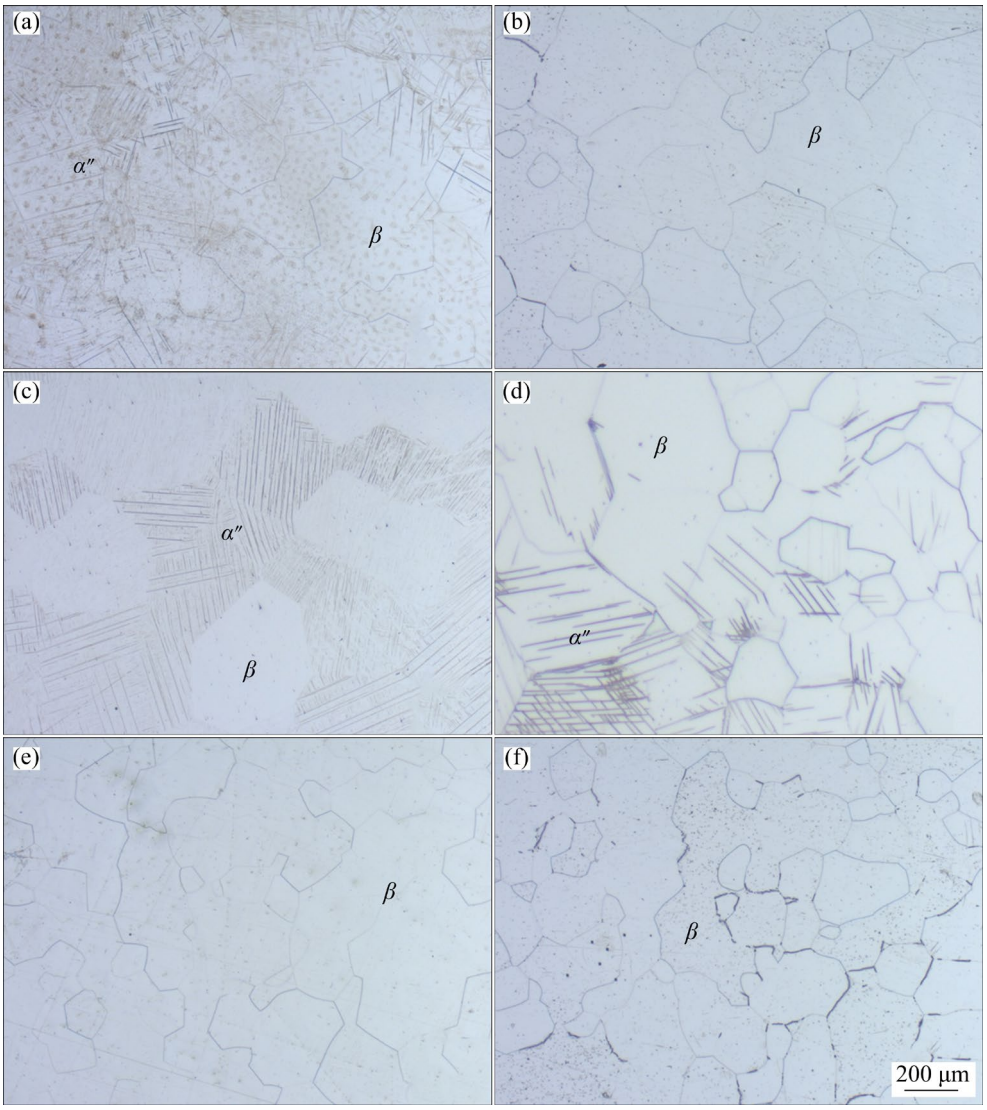

Fig. 3 Optical images of Ti−Nb−Cu shape memory alloys with different Cu contents: (a) 0.5 at.%; (b) 1.0 at.%; (c) 1.5 at.%; (d) 2.0 at.%; (e) 3.0 at.%; (f) 5.0 at.%

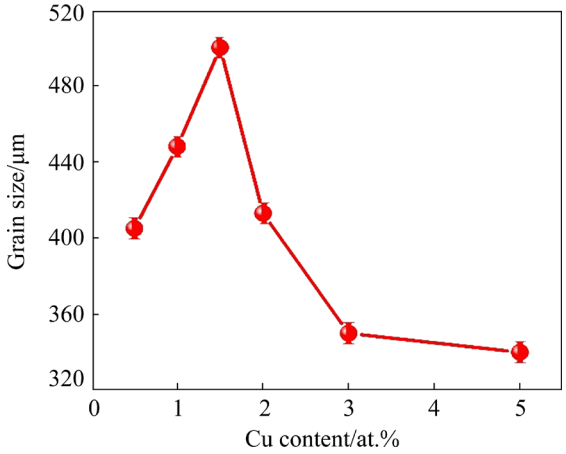

Fig. 4 Effect of Cu content on grain size of Ti−Nb−Cu shape memory alloys

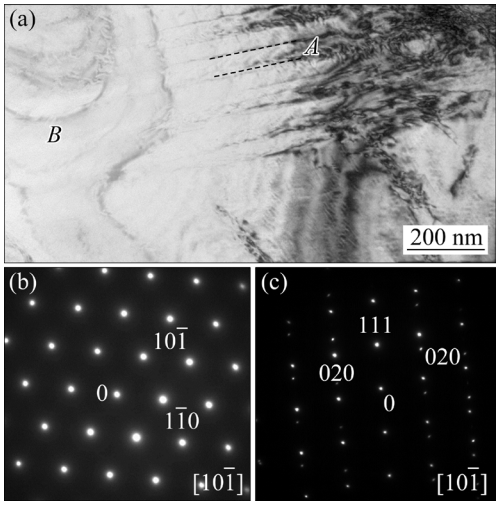

Fig. 5 Bright field TEM image (a) and corresponding SAED patterns (b, c) taken from Zones *A* and *B* in (a), respectively, for Ti−Nb-based shape memory alloys with 0.5 at.% Cu

and then decreases. As the Cu content increases from 0.5 at.% to 1.5 at.%, the mean grain size increases from 405 to 500 μm. When the content of Cu is more than 1.5 at.%, the grain size continuously decreases to 340 μm. This indicates that higher Cu content can play an important role in grain refinement. Similarly, it has been revealed that Al and Sn elements can also result in the reduction of grain size of Ti−Nb shape memory alloys [24−26].

Figure 5 shows the bright field TEM images and corresponding SAED patterns of Ti−Nb−$Cu_{0.5}$ shape memory alloys. As shown in Fig. 5(a), the cubic β parent phase and parallel α'' martensite phase coexist in the present Ti−Nb−Cu shape memory alloy, which can be verified by SAED patterns in Figs. 5(b) and (c). Moreover, the SAED pattern taken from Zone *B* further confirms that martensite lath is {111} type I twins related.

The bright field TEM image and the corresponding SAED pattern of Ti−Nb−$Cu_{1.0}$ shape memory alloy are shown in Fig. 6. It can be seen from Fig. 6(a) that the microstructure of Ti−Nb−Cu shape memory alloy is featured with the anonymous β austenite phase. However, in addition to the diffraction spot of β parent phase, some extra diffraction spots corresponding to ω phase are also detected. This means that the higher density ω phases exist in the β-phase matrix.

Similarly, β parent phase matrix modified by lots of ω phases is also found in Ti−Nb−$Cu_{1.5}$ shape memory alloy, which can be confirmed by TEM image in Fig. 7(a) and the corresponding SAED pattern in Fig. 7(b). Besides, it is found that the

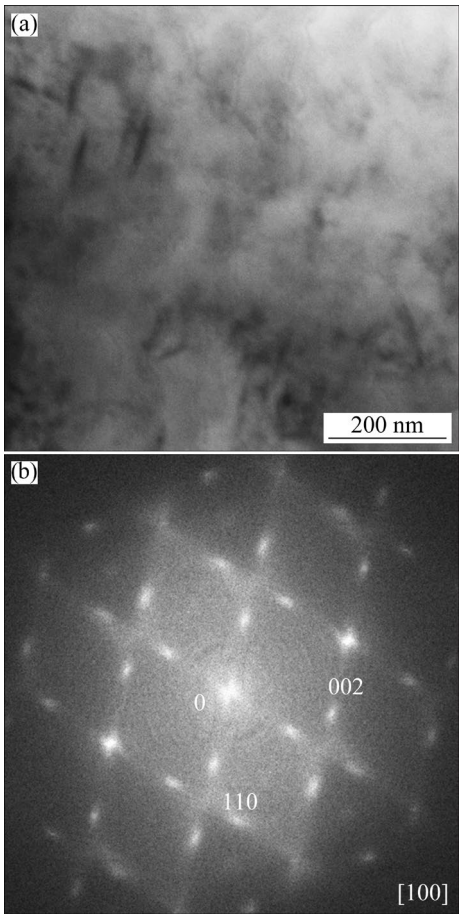

Fig. 6 Bright field TEM image (a) and corresponding SAED pattern (b) of Ti−Nb-based shape memory alloys with 1.0 at.% Cu

martensite lath coexists in the β parent phase matrix. The corresponding SAED pattern in Fig. 7(c) can further affirm the appearance of orthorhombic α''

martensite phase. Figure 7(d) represents the typical morphology of another area in Ti−Nb−$Cu_{1.5}$ shape memory alloy. Obviously, the typical self-accommodation martensite configuration with a V-shape and triangular shape is observed in Ti−Nb−$Cu_{1.5}$ shape memory alloy.

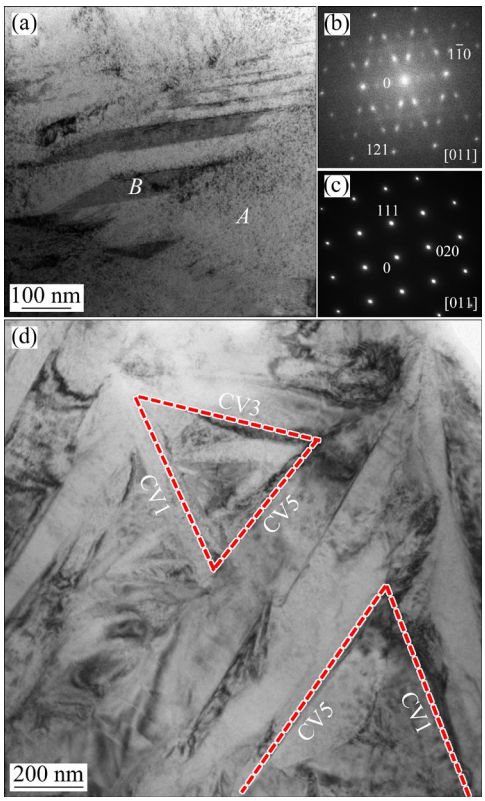

Fig. 7 Bright field TEM image (a) and corresponding SAED patterns (b, c) taken from Zones *A* and *B* in (a) for Ti−Nb-based shape memory alloys with 1.5 at.% Cu, respectively, and TEM image of another area (d) (CV*n* represents different martensite variants)

With further increasing Cu content to 2.0 at.%, both an orthorhombic α'' martensite phase and cubic β parent phase still coexist, as shown in Fig. 8(a). Differing from Ti−Nb−$Cu_{1.5}$ shape memory alloy, the corresponding SAED patterns in Figs. 8(b) and (c) indicate that ω precipitates completely disappear in Ti−Nb−$Cu_{2.0}$ shape memory alloy. Moreover, the tip of α'' martensite lath embeds into the β parent phase, which is consistent with the energy minimization theory. Similar to Ti−Nb−$Cu_{1.5}$ shape memory alloy, the V-shape martensite phase is still frequently observed in Ti−Nb−$Cu_{2.0}$ shape memory alloy.

As Cu content is up to 3.0 at.%, only featureless β parent phase matrix with a cubic structure is observed, while no martensite lath is detected in Ti−Nb−$Cu_{3.0}$ shape memory alloy, as shown in Fig. 9(a). Meanwhile, the single diffraction spots corresponding to β phase are detected in SAED pattern in Fig. 9(b) taken from Fig. 9(a). This implies that both ω precipitates and α'' martensite phase also fully disappear in Ti−Nb−$Cu_{3.0}$ shape memory alloy.

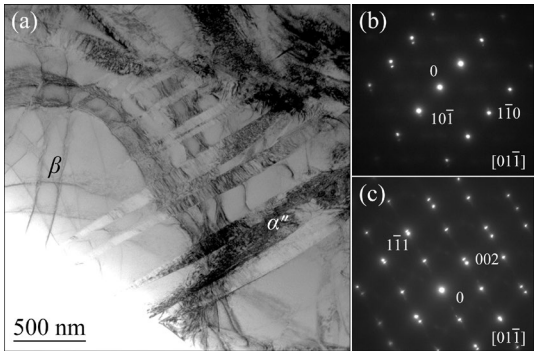

Fig. 8 Bright field TEM image (a) and corresponding SAED patterns taken from β (b) and α'' (c) zones of Ti−Nb-based shape memory alloys with 2.0 at.% Cu

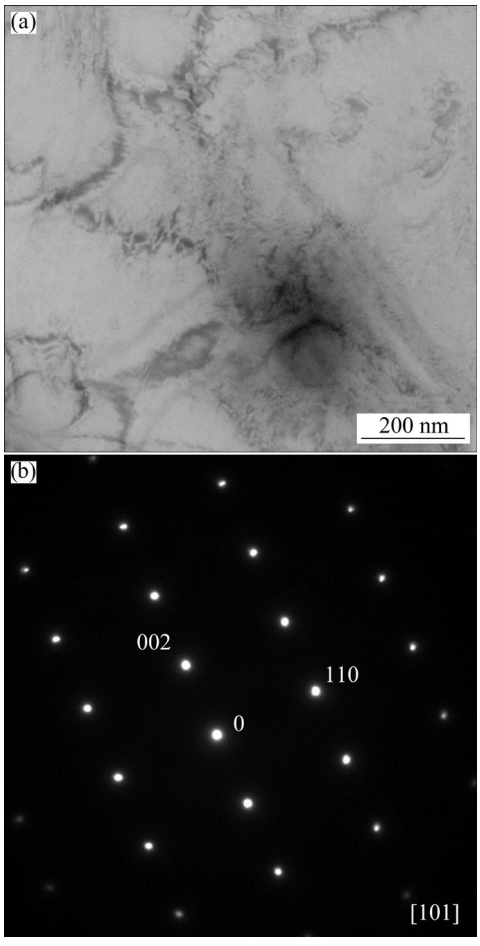

Fig. 9 Bright field TEM image (a) and corresponding SAED pattern (b) of Ti−Nb-based shape memory alloys with 3.0 at.% Cu

3.2 Martensitic transformation

For β-Ti-based shape memory alloys, there exists six orientation relationships between β phase and α'' martensite variants during martensitic transformation process, as listed in Table 1 [27,28].

Table 1 Orientation relationship between β phase and α'' martensite variants in martensitic transformation [27,28]

CVn	$[100]_{\alpha''}$	$[010]_{\alpha''}$	$[001]_{\alpha''}$
CV1	$[100]_{\beta}$	$[011]_{\beta}$	$[0\bar{1}1]_{\beta}$
CV2	$[\bar{1}00]_{\beta}$	$[0\bar{1}0]_{\beta}$	$[011]_{\beta}$
CV3	$[010]_{\beta}$	$[101]_{\beta}$	$[10\bar{1}]_{\beta}$
CV4	$[0\bar{1}0]_{\beta}$	$[10\bar{1}]_{\beta}$	$[101]_{\beta}$
CV5	$[001]_{\beta}$	$[110]_{\beta}$	$[\bar{1}10]_{\beta}$
CV6	$[00\bar{1}]_{\beta}$	$[\bar{1}10]_{\beta}$	$[110]_{\beta}$

As the basis vector of martensitic phase is regarded as the coordinate system, lattice transformation matrix ($\boldsymbol{T}_1'$) can be expressed as

$$\boldsymbol{T}_1'=\begin{bmatrix} a/a_0 & 0 & 0 \\ 0 & b/\sqrt{2}a_0 & 0 \\ 0 & 0 & c/\sqrt{2}a_0 \end{bmatrix} \tag{1}$$

When taking the base vector of the parent phase as the coordinate system, the lattice transformation matrix ($\boldsymbol{T}'$) can be indicated as

$$\boldsymbol{T}'=\boldsymbol{R}_1\boldsymbol{T}_1'\boldsymbol{R}_1^{\mathrm{T}} \tag{2}$$

where $\boldsymbol{R}_1$ expresses the transformation matrix of martensite variant transformation to parent phase; $\boldsymbol{R}_1^{\mathrm{T}}$ is the transpose of $\boldsymbol{R}_1$.

Taking martensitic variant CV1 as an example, based on the relationship between the martensite phase and parent phase $\boldsymbol{R}_1$ can be calculated as follows:

$$\boldsymbol{R}_1=\begin{bmatrix} 1 & 0 & 0 \\ 0 & 1/\sqrt{2} & -1/\sqrt{2} \\ 0 & 1/\sqrt{2} & -1/\sqrt{2} \end{bmatrix} \tag{3}$$

Hence, $\boldsymbol{T}'$ can be calculated by Eq. (2) as follows:

$$\boldsymbol{T}'=\begin{bmatrix} a/a_0 & 0 & 0 \\ 0 & (b+c)/(2\sqrt{2}\mathrm{a}_0) & (b-c)/(2\sqrt{2}\mathrm{a}_0) \\ 0 & (b-c)/(2\sqrt{2}\mathrm{a}_0) & (b+c)/(2\sqrt{2}\mathrm{a}_0) \end{bmatrix} \tag{4}$$

Plugging lattice constants of Ti−Nb−$Cu_{1.5}$ and Ti−Nb−$Cu_{2.0}$ in Fig. 2 into Eq. (4), $\boldsymbol{T}'$ can be obtained respectively as follows:

$$\boldsymbol{T}'_{\mathrm{Cu1.5}}=\begin{bmatrix} 0.9452 & 0 & 0 \\ 0 & 1.0109 & -0.0124 \\ 0 & -0.0124 & 1.0109 \end{bmatrix} \tag{5}$$

$$\boldsymbol{T}'_{\mathrm{Cu2.0}}=\begin{bmatrix} 0.9441 & 0 & 0 \\ 0 & 1.0141 & 0.0083 \\ 0 & 0.0083 & 1.0141 \end{bmatrix} \tag{6}$$

Lastly, we can obtain the lattice distortion matrix corresponding to six martensite variants, as listed in Table 2 and Table 3, respectively.

It has been reported that the martensite variants, which show a self-accommodation configuration, are frequently observed in β-Ti-based shape memory alloy in the previous literature, such as V-shape or triangular-shape [12,29]. Based on the energy minimization theory, multiple martensite

Table 2 Lattice distortion matrix of Ti−Nb−$Cu_{1.5}$ alloy for corresponding six lattice variants

CVn	$\boldsymbol{T}_i$	CVn	$\boldsymbol{T}_i$
CV1	$\begin{pmatrix} 0.9452 & 0 & 0 \\ 0 & 1.0109 & -0.0124 \\ 0 & -0.0124 & 1.0109 \end{pmatrix}$	CV2	$\begin{pmatrix} 0.9452 & 0 & 0 \\ 0 & 1.0109 & 0.0124 \\ 0 & 1.0109 & 0.0124 \end{pmatrix}$
CV3	$\begin{pmatrix} 1.0109 & 0 & 0.0124 \\ 0 & 0.9452 & 0 \\ 0.0124 & 0 & 1.0109 \end{pmatrix}$	CV4	$\begin{pmatrix} 1.0109 & 0 & -0.0124 \\ 0 & 0.9452 & 0 \\ -0.0124 & 0 & 1.0109 \end{pmatrix}$
CV5	$\begin{pmatrix} 1.0109 & 0.0124 & 0 \\ 0.0124 & 1.0109 & 0 \\ 0 & 0 & 0.9452 \end{pmatrix}$	CV6	$\begin{pmatrix} 1.0109 & -0.0124 & 0 \\ -0.0124 & 1.0109 & 0 \\ 0 & 0 & 0.9452 \end{pmatrix}$

Table 3 Lattice distortion matrix of Ti−Nb−$Cu_{2.0}$ alloy for corresponding six lattice variants

CVn	$\boldsymbol{T}_i$	CVn	$\boldsymbol{T}_i$
CV1	$\begin{pmatrix}0.9441 & 0 & 0\\ 0 & 1.0141 & 0.0083\\ 0 & 0.0083 & 1.0141\end{pmatrix}$	CV2	$\begin{pmatrix}0.9441 & 0 & 0\\ 0 & 1.0141 & -0.0083\\ 0 & 1.0141 & -0.0083\end{pmatrix}$
CV3	$\begin{pmatrix}1.0141 & 0 & -0.0083\\ 0 & 0.9441 & 0\\ -0.0083 & 0 & 1.0141\end{pmatrix}$	CV4	$\begin{pmatrix}1.0141 & 0 & 0.0083\\ 0 & 0.9441 & 0\\ 0.0083 & 0 & 1.0141\end{pmatrix}$
CV5	$\begin{pmatrix}1.0141 & -0.0083 & 0\\ -0.0083 & 1.0141 & 0\\ 0 & 0 & 0.9441\end{pmatrix}$	CV6	$\begin{pmatrix}1.0141 & 0.0083 & 0\\ 0.0083 & 1.0141 & 0\\ 0 & 0 & 0.9441\end{pmatrix}$

variants forming self-accommodation configuration can effectively minimize the transformation strain during the martensitic transformation. In addition, the martensite morphologies are largely dependent on the lattice distortion matrix ($\boldsymbol{T}_i$). Generally speaking, the lattice distortion matrix ($\boldsymbol{T}_i$) should immortally approach to unit matrix in order to achieve the lowest energy. It can be calculated that the combination of two martensite variants or three martensite variants can tend to unite matrix and further obtain the minimized energy. For instance,

$$\overline{\boldsymbol{T}}_{\text{V-shape}}=\frac{\boldsymbol{T}_1+\boldsymbol{T}_3}{2}=\begin{pmatrix}0.97805 & 0 & 0.0062\\ 0 & 0.97805 & -0.0062\\ 0.0062 & -0.0062 & 1.0109\end{pmatrix}\approx\begin{pmatrix}1&0&0\\0&1&0\\0&0&1\end{pmatrix} \quad (7)$$

$$\boldsymbol{T}'_{\text{Triangular}}=\frac{\boldsymbol{T}_1+\boldsymbol{T}_3+\boldsymbol{T}_5}{2}=\begin{pmatrix}0.9890 & 0.0041 & 0.0041\\ 0.0041 & 0.9890 & -0.0041\\ 0 & -0.0041 & 0.9890\end{pmatrix}\approx\begin{pmatrix}1&0&0\\0&1&0\\0&0&1\end{pmatrix} \quad (8)$$

The above results reveal that the martensite variants tend to show a V-shape or triangular morphologies in order to keep the minimum energy of the whole system, which is almost consistent with the TEM observations in Ti−Nb−$Cu_{1.5}$ and Ti−Nb−$Cu_{2.0}$ shape memory alloys.

It has been reported that the phase constituents of β-Ti-based shape memory alloys are largely dependent on two electronic parameters including the bond order ($\overline{\text{Bo}}$) and the metal d-orbital energy level ($\overline{\text{Md}}$) [17]. Figure 10 shows $\overline{\text{Bo}}-\overline{\text{Md}}$ diagram of Ti−Nb−Cu shape memory alloys with various Cu contents. Relationships between $\overline{\text{Bo}}$, $\overline{\text{Md}}$ and Cu content (x) can be expressed by the following equations:

$$\overline{\text{Md}}=2.44-0.019x \quad (9)$$

$$\overline{\text{Bo}}=2.8394-0.0073x \quad (10)$$

It can be found that adding Cu alloying element into Ti−Nb-based shape memory alloy results in the decrease of $\overline{\text{Bo}}$ and $\overline{\text{Md}}$. As Cu content increases from 0.5 at.% to 5.0 at.%, Ti−Nb−Cu shape memory alloys change from α'' martensite phase zone to β phase zone, crossing the boundary of $\beta/(\beta+\omega)$. Hence, martensite phase is observed in Ti−Nb−$Cu_{0.5}$ shape memory alloy. Adding 1.0 at.% Cu and 1.5 at.% Cu into Ti−Nb−Cu shape

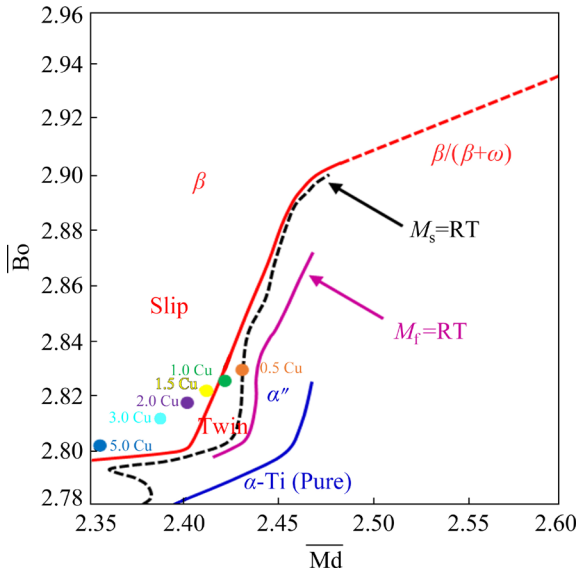

Fig. 10 $\overline{\text{Bo}}-\overline{\text{Md}}$ diagram for Ti−Nb-based shape memory alloys containing different Cu contents [17]

memory alloys makes them locate near the $\beta/(\beta+\omega)$ boundary, which leads to the precipitation of ω phase in the present Ti−Nb−Cu shape memory alloys. With further increasing Cu content to 3.0 at.% or 5.0 at.%, Ti−Nb−Cu shape memory alloys gradually become far away from the $\beta/(\beta+\omega)$ boundary, suppressing the precipitation of ω phase. This is almost consistent with the evolution of phase constituents in Ti−Nb−Cu shape memory alloy containing various Cu contents.

From the view point of microstructural evolution, it can be speculated that the martensitic transformation temperatures are closely related to Cu content in Ti−Nb-based shape memory alloys. For comparison, the martensitic transformation temperature of Ti−Nb−$Cu_{0.5}$ shape memory alloy is higher than that of Ti−Nb−$Cu_{1.0}$ shape memory alloy. Moreover, the martensitic transformation temperature of Ti−Nb−Cu shape memory alloy firstly increases and then decreases with further increasing Cu content from 1.0 at.% to 5.0 at.%. The variation of martensitic transformation temperature of Ti−Nb−Cu shape memory alloys can be attributed to the evolution of $\overline{Bo}$ and $\overline{Md}$.

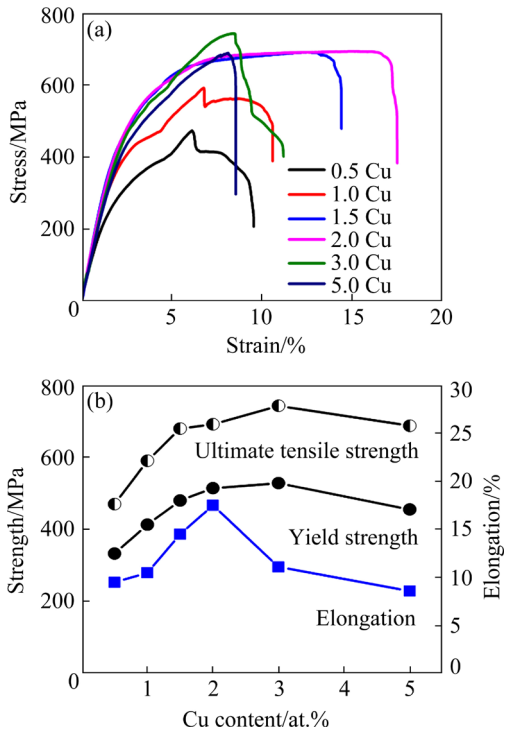

Fig. 11 Room temperature tensile stress−strain curves (a) and dependence of strength and elongation on Cu content (b) of Ti−Nb−Cu shape memory alloys

3.3 Mechanical properties

Figure 11(a) shows the room temperature tensile stress−strain curves of Ti−Nb−Cu shape memory alloys with various Cu contents. The results reveal that Cu content has an important influence on the mechanical properties of Ti−Nb−Cu shape memory alloys. The above XRD analysis and TEM observations reveal that all Ti−Nb−Cu shape memory alloys are mainly composed of β phase, regardless of the Cu content. Among them, Ti−Nb−Cu shape memory alloys with 0.5 at.% Cu and 1.0 at.% Cu have similar stress−strain curves, containing elastic deformation, stress-induced martensite transformation and elastic deformation of martensite phase. As the stress is up to the ultimate tensile stress, the samples are necked and failure. For Ti−Nb−Cu shape memory alloys with 1.5 at.% Cu and 2.0 at.% Cu, the elastic deformation of β phase, stress-induced martensite phase and last uniform plastic deformation are their primary deformation stages. The difference is that the plateaus of stress-induced martensite transformation and plastic deformation occur simultaneously in the Ti−Nb−Cu shape memory alloys with 1.5 at.% Cu and 2.0 at.% Cu. However, a significant work-hardening phenomenon is observed in tensile stress−strain curves of Ti−Nb−Cu shape memory alloys when the Cu content is more than 2.0 at.%. This may be related to more stable β parent phase in Ti−Nb−Cu shape memory alloys due to the higher Cu content. The mechanical properties of Ti−Nb−Cu shape memory alloys stemmed from Fig. 11(a) are shown in Fig. 11(b). Both the yield strength and ultimate tensile strength of Ti−Nb−Cu shape memory alloys increase rapidly, reaching the maximum values of 528 and 742 MPa at optimal 3.0 at.% Cu, respectively. This is obviously higher than those of other reported Ti−Nb-based shape memory alloys with Zr, Hf and Sn addition [29−35]. Combining with the microstructural analysis, the higher strength can be ascribed to the refined grain and solution strengthening. Further increasing the Cu content from 3.0 at.% to 5.0 at.% leads to a decrease of the yield strength and ultimate tensile strength. The elongation of Ti−Nb−Cu shape memory alloys also shows the same trend. The elongation of Ti−Nb−Cu shape memory alloy first increases from 9.5% to 17.5% and then decreases to 8.5% as the Cu content increases from 0.5 at.% to 2.0 at.% and then to

5.0 at.%. The superior elongation of 17.5% can be obtained in Ti−Nb−Cu shape memory alloy with tailoring 2.0 at.% Cu content. Compared with the Ti−Nb−$Cu_{1.5}$ shape memory alloy, there are not lots of ω precipitates in Ti−Nb−$Cu_{2.0}$ shape memory alloy. It is revealed that ω precipitates are brittle phase, which would deteriorate the ductility of β-Ti-based shape memory alloys [36,37]. While at Cu content exceeding 2.0 at.%, the Ti−Nb−Cu shape memory alloys are composed of more stable β parent phase, which is deformed by means of slip and is not favorable to the ductility. Thus, Ti−Nb−$Cu_{2.0}$ shape memory alloy possesses the excellent ductility as a result of the avoidance of ω precipitates and more stable β parent phase.

Figure 12 illustrates the tensile fracture surface images of Ti−Nb−Cu shape memory alloys with different Cu contents. On the whole, the fracture surface morphologies of all Ti−Nb−Cu shape memory alloys show the typical ductile fracture, which consist of dimples and tearing edges (directed by yellow arrow). Nevertheless, there exist some tiny differences among the Ti−Nb−Cu shape memory alloys with various Cu contents. For instance, the dimples of Ti−Nb−$Cu_{1.0}$ shape memory alloys are relatively flat. The size of dimples in Ti−Nb−$Cu_{1.5}$ shape memory alloy is significantly different in different zones. Besides, some discontinuous tearing edges are found at the bottom of individual dimples for Ti−Nb−$Cu_{5.0}$ shape memory alloy. That is the distinction of the fracture morphologies leading to the difference of elongation.

The influence of Cu content on the microhardness of Ti−Nb−Cu shape memory alloys is exhibited in Fig. 13. As seen, the microhardness of Ti−Nb−Cu shape memory alloys first increases and then decreases with increasing the Cu content. When the Cu content increases from 0.5 at.% to 1.5 at.%, the microhardness of Ti−Nb−Cu shape

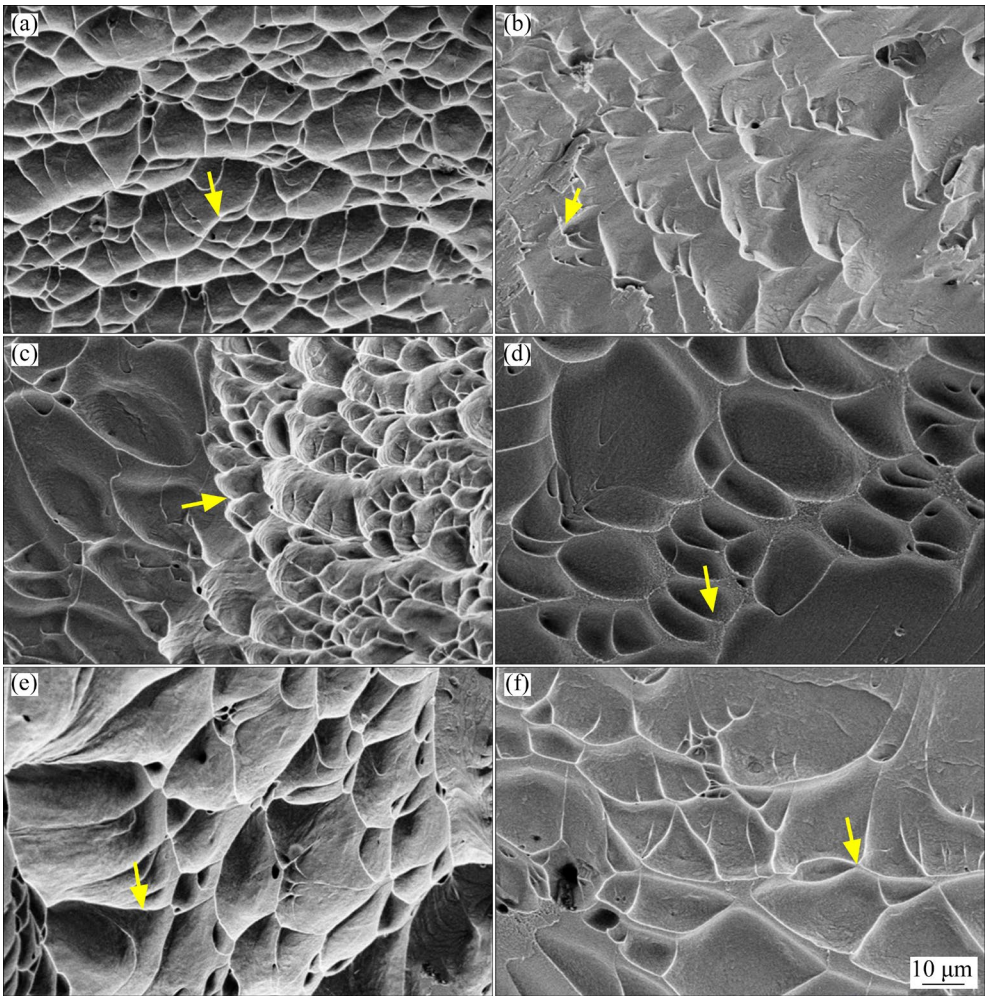

Fig. 12 SEM images showing fracture surface of Ti−Nb−Cu shape memory alloys with different Cu contents: (a) 0.5 at.%; (b) 1.0 at.%; (c) 1.5 at.%; (d) 2.0 at.%; (e) 3.0 at.%; (f) 5.0 at.%

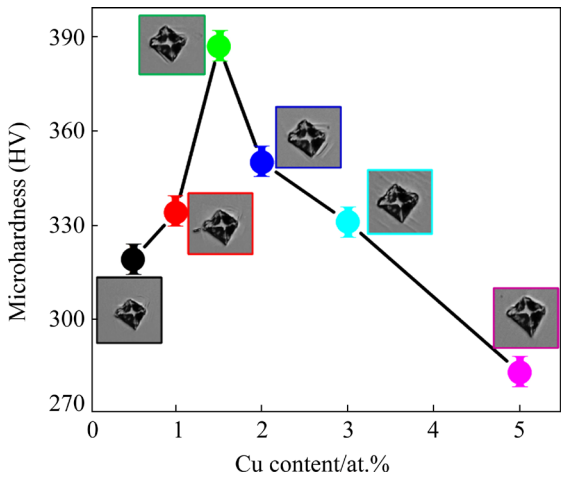

Fig. 13 Influence of Cu content on microhardness of Ti−Nb−Cu shape memory alloys

memory alloys increases from HV 319 to HV 387. Whereas, the microhardness decreases continuously to HV 283 when the content of Cu exceeds 1.5 at.%. The maximum microhardness of HV 387 can be obtained by adjusting Cu content of 1.5 at.%, which is obviously higher than that of Ti−Nb−O and Ti−Nb−Sn shape memory alloys [38,39]. The microhardness of β-Ti-based shape memory alloys can be controlled by solid solution strengthening, precipitation hardening, strain aging, grain size and phase compositions [39]. In the present Ti−Nb−Cu shape memory alloys, Cu addition can play an important role in solution strengthening. Moreover, the more the Cu content is, the more significant the strengthening effect is. In theory, the microhardness should continuously increase owing to the solution strengthening of Cu element. However, the precipitation strengthening is the more important factor in determining the micro-hardness, except for the solution strengthening. As stated in the above analysis, with increasing the Cu content, the amount of ω phase firstly increases and then decreases, further causing the first increase and then decrease of microhardness.

4 Conclusions

(1) The addition of Cu can tailor the phase constituents of Ti−Nb-based shape memory alloys. With increasing the Cu addition, both the $\overline{Bo}$ and $\overline{Md}$ monotonously decrease. In proportion, the evolution of phase constituents can be drawn as follows: $\beta+\alpha''\rightarrow\beta+\omega\rightarrow\beta+\alpha''+\omega\rightarrow\beta$.

(2) The grain size of Ti−Nb shape memory alloys firstly increases and then decreases with increasing Cu content.

(3) The martensite morphologies of Ti−Nb-based shape memory alloys with 1.5 at.% Cu and 2.0 at.% Cu show the typical self-accommodation configuration including V-shape and triangle.

(4) The yield strength, ultimate tensile strength and microhardness of Ti−Nb−Cu shape memory alloys firstly increase and then decrease. The Ti−Nb−Cu shape memory alloy with high performances containing the highest yield strength of 528 MPa and ultimate tensile strength of 742 MPa can be optimized by adding 3.0 at.% Cu, which is ascribed to the solution strengthening and grain refinement.

CRediT authorship contribution statement

Xiao-yang YI: Writing – Original draft, Conceptualization, Funding acquisition; **Xin-jian CAO:** Data curation, Writing – Review & editing; **Bo-wen HUANG:** Visualization, Investigation; **Kui-shan SUN** and **Bin SUN:** Data curation, Methodology and Investigation; **Xiang-long MENG and Zhi-yong GAO:** Resources, Project administration. **Hai-zhen WANG:** Funding acquisition and Writing – Review & editing.

Declaration of competing interest

The authors declare that they have no known competing financial interests or personal relationships that could have appeared to influence the work reported in this paper.

Acknowledgments

The authors are grateful for partial financial support from the National Natural Science Foundation of China (No. 52101231), the Science Fund of Shandong Laboratory of Yantai Advanced Materials and Green Manufacturing, China (No. AMGM2021F09), and the Natural Science Foundation of Shandong Province, China (No. ZR2021QE044).

References

[1] CUI Yan, LI Yan, LUO Kun, XU Hui-bin. Research progress on biomedical Ni-free Ti based shape memory alloys [J]. Rare Metal Materials and Engineering, 2010, 39(9): 1682−1686. (in Chinese)

[2] PATEL S K, BEHERA B, SWAIN B, ROSHAN R, SAHOO D, BEHERA A. A review on NiTi alloys for biomedical applications and their biocompatibility [J]. Materials Today:

Proceedings, 2020, 33: 5548−5551.

[3] TU Hai-ling, ZHAO Hong-bin, FAN Yan-yan, ZHANG Qing-zhu. Recent developments in nonferrous metals and related materials for biomedical applications in China: A review [J]. Rare Metals, 2022, 41: 1410−1433.

[4] SUN Bin, WANG Jun, MENG Xiang-long, WANG Jun. Size effect on the martensitic transformation of Ti−Nb shape memory alloy [J]. Intermetallics, 2022, 145: 107562.

[5] HASHIMOTO N, AL-ZAIN Y, YAMAMOTO A, KOYANO T, KIM H Y, MIYAZAKI. Novel beta-type high entropy shape memory alloys with low magnetic susceptibility and high biocompatibility [J]. Materials Letters, 2021, 257: 129286.

[6] SUN Kui-shan, SUN Bin, YI Xiao-yang, LI Hao, LI Xiang-yu, MENG Xiang-long, GAO Zhi-yong, CAI Wei. Influence of Er-doping on the microstructure and properties of β-Ti high temperature shape memory alloy [J]. Materials Characterization, 2022, 184: 111701.

[7] HASHMI M L, WADOOD A. Microstructural, mechanical and shape memory characterizations of Ti−Mo−Sn alloys [J]. Transactions of Nonferrous Metals Society of China, 2020, 30: 688−700.

[8] PARK M S, CHIU W T, NOHIRA N, TAHARA M, HOSODA H. Effects of Cr and Sn additives on the martensitic transformation and deformation behavior of Ti–Cr–Sn biomedical shape memory alloys [J]. Materials Science and Engineering: A, 2021, 822: 141668.

[9] CHIU W T, ISHIGAKI T, NOHIRA N, UMISE A, TAHARA M, HOSODA H. Effect of 3d transition metal additions on the phase constituent, mechanical properties, and shape memory effect of near-eutectoid Ti−4Au biomedical alloys [J]. Journal of Alloys and Compounds, 2021, 857: 157599.

[10] SOYKAN C. A theoretical approach to the structural, elastic and electronic properties of $Ti_{8-x}V_{4-y}Mo_{x+y+z}Al_{4-z}$ lightweight shape memory alloys for biomaterial implant applications [J]. Physica B: Condensed Matter, 2020, 598: 412416.

[11] SUN Bin, SUN Kui-shan, MENG Xiang-long, CAI Wei. Effect of texture on shape memory property of Ti−16Nb high temperature shape memory alloy [J]. Materials Science and Engineering: A, 2021, 809: 140779.

[12] SUN Bin, MENG Xiang-long, GAO Zhi-yong, CAI Wei. Effect of annealing temperature on shape memory effect of cold-rolled Ti−16at.%Nb alloy [J]. Journal of Alloys and Compounds, 2017, 715: 16−20.

[13] LI Qiang, HUANG Qi, LI Jun-Jie, HE Qian-feng, NAKAI M, ZHANG Ke, NIINOMI M, YAMANAKA K, CHIBA A, NAKANO T. Microstructure and mechanical properties of Ti–Nb–Fe–Zr alloys with high strength and low elastic modulus [J]. Transactions of Nonferrous Metals Society of China, 2022, 32: 503−512.

[14] KIM H Y, MIYAZAKI S. Several issues in the development of Ti−Nb-based shape memory alloys [J]. Shape Memory Superelasticity, 2016, 2: 380−390.

[15] GUO Shun, MENG Qing-kun, LIAO Guang-yue, HU Liang, ZHAO Xin-qing. Microstructural evolution and mechanical behavior of metastable β-type Ti−30Nb−1Mo−4Sn alloy with low modulus and high strength [J]. Progress in Natural Science: Materials International, 2015, 25: 414−418.

[16] ZHOU Ying-long, NIINOMI M, AKAHORI T. Effects of Ta content on Young's modulus and tensile properties of binary Ti−Ta alloys for biomedical applications [J]. Materials Science and Engineering: A, 2004, 371: 283−290.

[17] ABDEL-HADY M, HINOSHITA K, MORINAGA M. General approach to phase stability and elastic properties of β-type Ti-alloys using electronic parameters [J]. Scripta Materialia, 2006, 55: 477−480.

[18] SAITO T, FURUTA T, HWANG J H, KURAMOTO S, NISHINO K, SUZUKI N, CHEN R, YAMADA A, ITO K, SENO Y, NONAKA T, IKEHATA H, NAGASAKO N, IWAMOTO C, IKUHARA Y, SAKUMA T. Multifunctional alloys obtained via a dislocation-free plastic deformation mechanism [J]. Science, 2003, 300: 464−467.

[19] ZHANG Er-lin, FU Shan, WANG Ruo-xian, LI Hai-xia, LIU Ying, MA Zhi-qiang, LIU Guang-kun, ZHU Chen-shun, QIN Gao-wu, CHEN Da-fu. Role of Cu element in biomedical metal alloy design [J]. Rare Metals, 2019, 38: 476−494.

[20] SUN Kui-shan, YI Xiao-yang, SUN Bin, YIN Xing-he, MENG Xiang-long, CAI Wei, ZHAO Lian-cheng. Microstructure and mechanical properties of Ti−V−Al−Cu shape memory alloy by tailoring Cu content [J]. Materials Science and Engineering: A, 2020, 771: 138641.

[21] CHEN Cheng, FENG Xiao-mei, SHEN Yi-fu. Microstructure and mechanical properties of Ti−Cu amorphous coating synthesized on pure Cu substrate by mechanical alloying method [J]. Rare Metals, 2020, 39: 1222−1228.

[22] MA Zheng, YAO Min, LIU Rui, YANG Kai-min, REN Ling, ZHANG Yu, LIAO Zuo, LIU Wei, QI Ming. Study on antibacterial activity and cytocompatibility of Ti−6Al−4V−5Cu alloy [J]. Materials Technology, 2015, 30: B80−B85.

[23] CHIU W, WAKABAYASHI K, UMISE A, TAHARA M, HOSODA H. Enhancement of mechanical properties and shape memory effect of Ti−Cr-based alloys via Au and Cu modifications [J]. Journal of the Mechanical Behavior of Biomedical Materials, 2021, 123: 104707.

[24] TAKAHASHI E, SAKURAI T, WATANABE S, MASAHASHI N, HANADA S. Effect of heat treatment and Sn content on superelasticity in biocompatible Ti−Nb−Sn alloys [J]. Materials Transactions, 2002, 43: 2978−2983.

[25] FAROOQ M U, KHALID F A, ZAIGHAM H, ABIDI I H. Superelastic behaviour of Ti−Nb−Al ternary shape memory alloys for biomedical applications [J]. Materials Letters, 2014, 121: 58−61.

[26] WANG Ben-li, ZHENG Yu-feng, ZHAO Liang-cheng. Effects of Sn content on the microstructure, phase constitution and shape memory effect of Ti−Nb−Sn alloys [J]. Materials Science and Engineering: A, 2008, 486: 146−151.

[27] CHAI Y W, KIM H Y, HOSODA H, MIYAZAKI S. Self-accommodation in Ti−Nb shape memory alloys [J]. Acta Materialia, 2009, 57: 4054−4064.

[28] INAMURA T, YAMAMOTO Y, HOSODA H, KIM H Y, MIYAZAKI S. Crystallographic orientation and stress-amplitude dependence of damping in the martensite phase in textured Ti–Nb–Al shape memory alloy [J]. Acta Materialia, 2010, 58: 2535−2544.

[29] SUN Bin, MENG Xiang-long, GAO Zhi-yong, CAI Wei. Martensitic transformation and shape memory effect of Ti−16Nb−xZr (x=0−8) alloys [J]. Physics of Metals and Metallography, 2019, 120: 750−755.

[30] RAMALOHARY A, CASTANY P, LAHEURTE P, PRIMA F, GLORIANT T. Superelastic property induced by low-temperature heating of a shape memory Ti−24Nb−0.5Si biomedical alloy [J]. Scripta Materialia, 2014, 88: 25−28.
[31] BRAILOVSKI V, PROKOSHKIN S, GAUTHIER M, INAEKYAN K, DUBINSKIY S. Mechanical properties of porous metastable beta Ti–Nb–Zr alloys for biomedical applications [J]. Journal of Alloys and Compounds, 2013, 577(Suppl.): 413−417.
[32] YANG R, RAHMAN K M, RAKHYMBERDIYEV A N, DYE D, VORONTSOV V A. Mechanical behaviour of Ti−Nb−Hf alloys [J]. Materials Science and Engineering: A, 2019, 740/741: 398−409.
[33] ZHOU Yu, LI Yu-xuan, YANG Xian-jin, CUI Zhen-duo, ZHU Sheng-li. Influence of Zr content on phase transformation microstructure and mechanical properties of $Ti_{75-x}Nb_{25}Zr_x$ (x=0.6) alloys [J]. Journal of Alloys and Compounds, 2009, 486: 628−632.
[34] IBRAHIM M K, HAMZAH E, SAUD S N. Microstructure, phase transformation, mechanical behavior, bio-corrosion and antibacterial properties of Ti−Nb−xSn (x=0, 0.25, 0.5 and 1.5) SMAs [J]. Journal of Materials Engineering and Performance, 2019, 28: 382−393.
[35] EHTEMAM-HAGHIGHI S, LIU Yu-jing, CAO Guang-hui, ZHANG Lai-chang. Phase transition, microstructural evolution and mechanical properties of Ti−Nb−Fe alloys induced by Fe addition [J]. Materials & Design, 2016, 97: 279−286.
[36] LI Shuang-lei, CHOI M S, NAM T H. Role of fine nanoscaled isothermal omega phase on the mechanical and superelastic properties of a high Zr-containing Ti−Zr−Nb−Sn shape memory alloy [J]. Materials Science and Engineering: A, 2020, 782: 139278.
[37] CHENG Jun, LI Jin-shan, YU Sen, DU Zhao-xin, ZHANG Xiao-yong, ZHANG Wen, GAI Jin-yang, WANG Hong-chuan, SONG Hong-jie, YU Zhen-tao. Influence of isothermal ω transitional phase-assisted phase transition from β to α on room-temperature mechanical performance of a meta-stable β titanium alloy Ti−10Mo−6Zr−4Sn−3Nb (Ti−B12) for medical application [J]. Frontiers in Bioengineering and Biotechnology, 2021, 8: 1518.
[38] MORAES P E L, CONTIERI R J, LOPES E S N, ROBIN A, CARAM R. Effects of Sn addition on the microstructure, mechanical properties and corrosion behavior of Ti–Nb–Sn alloys [J]. Materials Characterization, 2014, 96: 273−281.
[39] WANG Jun-shuai, XIAO Wen-long, REN Lei, FU Yu, MA Chao-li. The roles of oxygen content on microstructural transformation, mechanical properties and corrosion resistance of Ti−Nb-based biomedical alloys with different β stabilities [J]. Materials Characterization, 2021, 176: 111122.

基于 d 电子理论的 Ti−Nb−Cu 三元形状记忆合金性能优化

衣晓洋[1]，曹新建[2]，黄博文[3]，孙嵚善[3]，孙 斌[4]，孟祥龙[3]，高智勇[3]，王海振[1]

1. 烟台大学 核装备与核工程学院，烟台 264005；
2. 山东省烟台先进材料与绿色制造实验室，烟台 264005；
3. 哈尔滨工业大学 材料科学与工程学院，哈尔滨 150001；
4. 哈尔滨工程大学 材料科学与化学工程学院 分析测试中心，哈尔滨 150001

摘 要：基于 d 电子理论设计 Ti−Nb−Cu 形状记忆合金的相组成，以优化其性能。XRD 分析和 TEM 观察表明，Cu 添加导致键级($\overline{Bo}$)和金属 d 轨道能级($\overline{Md}$)值减小，从而使相组成发生演变。随着 Cu 含量的增加，相组成的变化可以总结如下：$\beta+\alpha''\rightarrow\beta+\omega\rightarrow\beta+\alpha''+\omega\rightarrow\beta$。随着 Cu 含量的增加，Ti−Nb−Cu 形状记忆合金的屈服强度、极限抗拉强度和伸长率均呈先增大后减小的趋势。通过优化 Cu 合金元素含量，Ti−Nb−Cu 形状记忆合金具有优异的力学性能，其屈服强度为 528 MPa，极限抗拉强度为 742 MPa，这主要归因于固溶强化、晶粒细化以及析出强化的综合作用。

关键词：d 电子理论；Ti−Nb−Cu 形状记忆合金；马氏体组态；拉伸性能；显微硬度

(Edited by Wei-ping CHEN)